HHS Public Access

Author manuscript

J Mech Behav Biomed Mater. Author manuscript; available in PMC 2020 July 01.

Published in final edited form as:

J Mech Behav Biomed Mater. 2019 July ; 95: 13–20. doi:10.1016/j.jmbbm.2019.03.024.

Biomechanical test protocols to detect minor injury effects in intervertebral discs

Olivia M. Torre, **Thomas W. Evashwick-Rogler**, **Phillip Nasser**, **James C. Iatridis***

Leni & Peter W. May Department of Orthopaedics, Icahn School of Medicine at Mount Sinai, One Gustave Levy Place, Box 1188, New York, NY, 10029-6574, USA

Abstract

Intervertebral discs (IVDs) maintain flexibility of the spine and bear mechanical load. Annulus fibrosus (AF) defects are associated with IVD degeneration and herniation which disrupt biomechanical function and can cause pain. AF puncture injuries can induce IVD degeneration but are needed to inject therapies. Identifying small AF defects with biomechanical testing can be difficult because IVDs have a complex, composite structure and nonlinear biomechanical properties that are dependent on AF fiber tension. It remains unclear how choice of biomechanical testing protocols affect the sensitivity of biomechanical properties to AF injuries. This study determined whether axial preload or magnitude of cyclic axial or torsional testing affected the ability to detect minor AF defects in rat caudal motion segments using *ex vivo* biomechanical testing. Intact and injured motion segments were subjected to a repeated measures study design with multiple biomechanical testing protocols that varied axial tension-compression force amplitude (± 1.6 N, ± 8.0 N, ± 16.0 N), axial preload (−1.6 N, −8.0 N, −16.0 N, corresponding to −0.1 MPa, −0.5 MPa, and −1.0 MPa, respectively), and torsional rotation angle (± 10°, ± 15°, and ± 20°). Biomechanical properties obtained from the lowest force testing conditions for axial tension-compression (± 1.6 N), axial preload (−1.6 N), and angular rotation (± 10°) exhibited the largest differences in biomechanical properties between intact and injured conditions. Biomechanical properties determined under low axial force or torsion amplitudes involve less AF fiber tension and were most sensitive to injury. Low force testing protocols are recommended for detecting minor structural AF defects and may enable more precise assessments of IVD injuries, healing or repair.

Keywords

Intervertebral disc; Motion segment biomechanics; Biomechanical test protocol; Needle puncture injury; IVD degeneration; IVD repair

*Corresponding author. james.iatridis@mssm.edu (J.C. Iatridis).

Declarations of interest

None.

1. Introduction

Back pain is a leading cause of global disability (Hoy et al., 2014; Centers for Disease Control and Prevention (CDC), 2009; D 2016 Disease and Inju, 2017), and is associated with IVD degeneration (Livshits et al., 2011). The annulus fibrosus (AF) of the intervertebral disc (IVD) is a complex hierarchical tissue consisting of collagen fibers that function to contain the inner nucleus pulposus (NP) and connect adjacent vertebrae during spinal loading (Cortes et al., 2014; Iatridis et al., 2013). AF defects accumulate during aging and degeneration, and AF injuries can result in loss of AF fiber tension and NP herniation with consequential biomechanical changes that contribute to painful conditions (Adams and Roughley, 2006). IVD degeneration can result in back pain due to structural damage occurring in the AF and endplates (Adams and Dolan, 2012). Large and small AF defects have been shown to accelerate IVD degeneration and height loss (Iatridis et al., 2006, 2013; Elliott et al., 2008) and can lead to vascularization and innervation (Melrose et al., 2002; Freemont et al., 1997). Annular tears are implicated with age, degeneration, and impaired motion segment mechanics (Livshits et al., 2011; Thompson et al., 2000, 2004; Osti et al., 1992; Fazzalari et al., 2001). Adult IVDs heal poorly (Hampton et al., 1989; Martin et al., 2013; Torre et al., 2018), and the limited IVD healing that does occur is most likely to occur at early stages of injury when defects remain small. Tissue engineering and regenerative medicine techniques show most promise when applied early to minor IVD defects. A need has arisen to develop increasingly precise biomechanical test protocols capable of detecting functionally important biomechanical changes due to small IVD injuries and healing responses.

Improved biomechanical function is an important design criteria of IVD repair strategies (Long et al., 2016). There is a growing need to identify biomechanical test protocols and can identify small AF injuries and more subtle defects since biological repair strategies are being developed for implementation at early degeneration states or minor injuries. AF needle puncture injuries are the most commonly used acute injury in animal models of IVD herniation and degeneration. AF needle puncture results in altered *ex vivo* motion segment biomechanical behaviors and instability as well as cellular and biochemical changes representative of IVD degeneration (Elliott et al., 2008; Michalek et al., 2010a; Michalek and Iatridis, 2012; Masuda et al., 2005; Iatridis et al., 2009; Hartman et al., 2015; Sobajima et al., 2005). Needle puncture and injection is known to cause IVD degeneration in discography procedures, and is also a likely route for regenerative medicine treatments (Carragee et al., 2009; van Heeswijk et al., 2018; Iatridis and Hecht, 2012). Thus, AF puncture injury models are widely adopted to assess the potential of experimental strategies to repair injured IVDs in both large and small animal models (Sloan et al., 2018). Even small AF defects result in significant alteration of microscale behavior in the AF and initiate biomechanical and biological changes suggestive of degeneration (Iatridis et al., 2009; Michalek et al., 2010b). The ability to detect small AF defects using *ex vivo* motion segment mechanical testing requires refined test protocols. In contrast, large, AF defects are commonly detected regardless of loading protocol. It is unknown if the ability to detect differences in mechanical behavior between intact and injured IVDs is affected by the magnitude of axial and torsional displacements applied during biomechanical testing or the

axial preload prior to testing, which can both influence the amount of AF tension and NP pressurization. We believe that biomechanical testing protocols and parameters can be adjusted to best reveal structural defects and increase sensitivity of injury detection.

While *ex vivo* biomechanical testing methods are commonly used to measure IVD functional behaviors, there is a lack of uniformity of biomechanical testing protocols which creates a challenge when comparing across different studies. The choice of testing protocol on vertebra-IVD-vertebra motion segments *ex vivo* can alter biomechanical parameters. Testing methods vary in terms of test modality (e.g., axial, torsional, bending, complex loading), specific test protocols, and analysis methods. These inconsistencies have potential to influence parameter estimation and/or interpretation of outcomes, and are especially important when comparing more subtle effects expected with mild degeneration, small IVD defects, or when comparing different IVD repair strategies. IVD biomechanical behaviors are non-linear due to of non-linear material properties and because of complex structural interactions between NP and AF. The NP contributes more to load carriage than the AF at lower loads (Johannessen et al., 2006), while the AF experiences more radial stresses at higher loads (Adams et al., 1996; Costi et al., 2007; O'Connell et al., 2011). Therefore, motion segment biomechanical responses are influenced by loading levels which can be adjusted to simulate physiological levels by altering the test protocol. The IVD experiences a resting compressive stress *in vivo* due to activation of surrounding spinal muscles, and the application of an axial preload *ex vivo* can stimulate these physiological conditions and increase IVD axial and torsional stiffness and hysteresis (Gardner-Morse and Stokes, 2003, 2004). Further, torsional mechanical properties are most sensitive to AF integrity, and these properties change nonlinearly with rotation angle (Bezci et al., 2018).

The objective of this study was to determine mechanical testing protocols that best detected small IVD injuries in rat caudal IVDs. Rat caudal IVDs were used because of their simplified geometry and common use in puncture animal models (Lai et al., 2015; Sloan et al., 2017; Rousseau et al., 2007; Ulrich et al., 2007). Rat caudal IVDs were evaluated with cyclic axial and torsional biomechanical tests with varying axial loading amplitude, axial preload value, and torsional rotation angle amplitude. Stiffness, range of motion, neutral zone and hysteresis parameters were calculated. Results demonstrated that small AF defects were most sensitively detected when tested under relatively low load magnitude, low axial preload, and fewer degrees of rotation.

2. Materials and methods

2.1. Animals and specimen preparation

Motion segments from skeletally mature Sprague Dawley rats (n = 10) from coccygeal levels c4/5, c6/7 and c8/9 were dissected for a total of 30 motion segments with intact rostral and caudal vertebrae, wrapped in 1X PBS soaked Kim wipes and stored at −20 °C until day of testing. Motion segments from multiple levels were evenly distributed between three axial preload groups to control for potential level effects, although geometry of rat caudal IVDs is similar (Espinoza Orías et al., 2009). Axial preloads of −1.6 N, −8.0 N and −16.0 N corresponding to −0.1 MPa, −0.5 MPa, and −1.0 MPa (calculated as load/area), respectively, were chosen as they correspond approximately to intradiscal pressures while lying prone,

relaxed standing, and sitting with knees flexed (Wilke et al., 1999). On the day of testing, motion segments were thawed in 1X PBS at room temperature for 2 h and excess connective tissue was removed using a scalpel. Motion segments were visually aligned in custom stainless steel pots using a plumb line and pottted using an instant adhesive (Loctite 401, Henkel, Düsseldorf, Germany) with an accelerant (Loctite 712, Henkel, Düsseldorf, Germany).

2.2. Study design and annular puncture injury

A repeated measures study design was used where motion segments first underwent testing in the intact condition followed by rehydration, injury, and re-testing (Fig. 1A). Following axial and torsional testing (described below) in the intact condition, minor injury was induced using a dorsolateral puncture injury with a 26 gauge (G) syringe needle tip. The 26G syringe needle (0.46 mm outer diameter) created an injury of approximately 40% of average rat caudal IVD height of 1.16 mm (Hsieh et al., 2009), and this size corresponds to minor injury since it was previously shown to induce IVD degeneration but biomechanical testing demonstrated puncture injuries of 40% or less had variable effects and were difficult to detect (Elliott et al., 2008). This injury is also considered minor because no herniation occurred as determined by visual inspection, and the syringe needle tip used to create the injury is sharp and beveled, simulating annular tears as opposed to a biopsy or box defect. Injured IVDs were placed in 1X PBS for 60 min to rehydrate, and then retested in the injured condition. This repeated measures study design allowed determination of specimen matched biomechanical parameters in intact and injured conditions.

2.3. Axial and torsional loading

Axial tension-compression testing was performed using an Enduratec ELF 3200 (TA Instruments, New Castle, DE) using a force-controlled cyclic testing protocol. Potted motion segments were secured in the testing machine and loaded at three different magnitudes for 20 cycles per magnitude at a frequency of 1 Hz: ± 1.6 N, ± 8.0 N, and ± 16.0 N (Fig. 1B). After axial tension-compression testing, motion segments were allowed to free swell in PBS for 30 min. Torsional testing was performed using an AR2000ex rheometer (TA instruments, New Castle, DE) using an angular displacement-controlled cyclic testing protocol. The torsional testing protocol was comprised of two stages: 1) axial compressive preload and 2) cyclic angular rotation. Potted motion segments were secured in the testing machine, and axial compressive preload was first applied for 5 min at one of three magnitudes: ± 1.6 N, ± 8.0 N, or ± 16.0 N and then held at steady displacement for torsion loading (Fig. 1C). Samples were then rotated to three different angular displacement magnitudes for 20 cycles each at a frequency of 1 Hz: ± 10°, ± 15°, and ± 20°. Increasing load magnitudes for axial testing or angles of rotation for torsional testing were selected to reflect the loading curve under varying levels of challenge to the motion segment-from least challenging where the loading curve does not reach linearity, to most challenging where the loading curve reaches the linear region (Fig. 1D).

2.4. Biomechanical parameter evaluation

Axial data were analyzed for compressive stiffness, tensile stiffness, range of motion (ROM) and neutral zone (NZ) length (Fig. 2A), and torsional data were analyzed for torsional

stiffness, torque range, NZ length, and hysteresis (Fig. 2B) from the last cycle of testing (Martin et al., 2013; Johannessen et al., 2006; Beckstein et al., 2008) for each test by using a custom MATLAB (MathWorks, Natick MA) code.

Compressive and tensile stiffness was calculated as the slope of the top and bottom 20% of the load vs. displacement curves, respectively. Axial ROM was calculated as the total displacement from compression to tension. Torsional stiffness in the clockwise and counterclockwise directions was averaged to obtain a single torsional stiffness value. Torsional stiffness was calculated as the average of the top 20% of the torque vs. rotation curve in both the clockwise and counterclockwise rotations. Torque range was calculated as the total torque developed from the fully counterclockwise to fully clockwise rotations. Axial and torsional NZ length was defined as the displacement or rotation for which 0 load is developed (Panjabi, 1992) and was manually determined from the load vs. displacement or torque vs. rotation plots using a custom MATLAB script, and values were taken as the average NZ measurements from 3 users. The average ICC for manually determined axial NZ length of three users was ICC = 0.9568.

A custom MATLAB script was developed to automate NZ length measurements, reduce human variability, and decrease analyses time. Torsional torque-displacement curves were used to compare manually obtained NZ lengths and NZ lengths obtained using the automated method. Automated torsional NZ length was identified from the last complete cycle of loading using a custom algorithm written in MATLAB that calculated the slope of the nonlinear regions with lowest stiffness and little curvature. Briefly, the region of smallest slope was found by linear regression of a short segment that was moved along the entire length of the force-displacement curve. This initial segment length was chosen by visual estimation to be a small portion of the neutral zone with negligible curvature. The standard error of the fit provides a baseline value that characterized the sampled data noise. The length of this small segment was then expanded independently in both positive and negative directions until the standard error had increased by 15% over the base value to indicate an increase in curvature. The NZ lengths were calculated as the length of this line where the threshold was met.

2.5. Statistical analyses

Statistical analyses were performed using Prism (GraphPad, La Jolla, CA) taking $p < 0.05$ to be significant. All data were confirmed as normally distributed using the Shapiro-Wilk Normality test. Two-way ANOVA with Sidak's multiple comparison test determined the effects of acute injury and loading condition on axial and torsional biomechanical parameters. Two-way ANOVA with Tukey's multiple comparison test determined the effect of axial preload and rotation amplitude in torsional testing on percent change from intact conditions. Inter-class correlation coefficient (ICC) was determined from axial NZ length measurements of three users. The Pearson's correlation coefficient (r) and coefficient of determination (r^2) were calculated to determine the correlation between manually calculated and automated NZ lengths. G*Power 3.1 was used to determine the statistical power of the correlation test using an effect size of 0.9574, as calculated from the coefficient of determination from the correlation of 14 randomly selected samples. The calculated power

was 1.0, indicating a low probability of type II error using 14 samples for the correlation analysis.

3. Results

3.1. Compressive stiffness and axial range of motion were sensitive to minor annular injury at a relatively low load magnitude

Minor injury resulted in a significantly reduced compressive stiffness compared to the intact condition at the lowest axial loading magnitude of ± 1.6N, with no changes detected at higher loading magnitudes or between axial loading magnitude groups (Fig. 3A). Minor injury resulted in a significant reduction in tensile stiffness at the lowest axial loading magnitude of ± 1.6N with no change at higher loading magnitudes or between axial loading groups (Fig. 3B). Minor injury resulted in significantly increased range of motion was significantly increased for all axial loading magnitudes, but the effect was most pronounced at ± 1.6N (Fig. 3C). Axial NZ length was only significantly increased at the lowest loading magnitude of ± 1.6N, with a trend ($p < 0.1$) of a greater effect compared to the highest loading magnitude of ± 16N (Fig. 3D). Intact compressive stiffness, tensile stiffness, range of motion, and axial NZ length increased with load magnitude, and the parameter with the greatest % change detected between intact and injury was axial range of motion at the lowest loading magnitude of ± 1.6N at 49.18% change (Table 1).

3.2. Torsional stiffness and torque range were sensitive to minor annular injury at a relatively low axial preload with smaller rotational angle

Torsional stiffness was significantly decreased with injury compared to intact for all experimental groups of varying axial preload and degrees of rotation. The lowest axial preload of 1.6N combined with the fewest degrees of rotation of ± 10° exhibited the largest percent difference of injury on torsional stiffness (Fig. 4A). Torque range was also significantly decreased with injury in all groups, with the largest differences from intact at the lowest loading conditions of 1.6N axial preload for ± 10° and ± 15° compared to the highest axial preload of ± 16N combined with the most degrees of rotation of ± 20° (Fig. 4B). Intact values for torsional stiffness and torque range increased with increasing axial preload and rotation amplitude. The parameter with the greatest % change detected between intact and injury was torsional stiffness at 1.6N axial preload combined with ± 10° with a 34.1% change (Table 2).

3.3. Torsional neutral zone length and hysteresis were insensitive to minor injury

Torsional NZ length and hysteresis were unaffected by injury for all groups, although trends ($p < 0.1$) were observed at 16N combined with ± 15° rotation and 1.6N combined with ± 25° rotation, respectively (Fig. 4C and D). Torsional NZ length and hysteresis were less sensitive to injury compared to torsional stiffness and torque range, which may be been partly related to greater variability since values for percent change in NZ from intact values are lower than for stiffness and torque range (Fig. 4). Mean values of torsional neutral zone length increased with injury as expected, although this was not significant so we conclude torsional NZ length was insensitive to minor injury or loading protocol (Fig. 4C, Table 3). Similarly, mean values of hysteresis were decreased with injury in all groups, although this was not

significant, therefore torsional hysteresis was insensitive to minor injury or loading protocol (Fig. 4D, Table 3).

The correlation coefficient and coefficient of determination of torsional NZ lengths obtained manually and via an automated MATLAB script was determined. A correlation analysis of NZ length measurements of 14 randomized samples from our total data set determined the correlation coefficient of manual NZ length measurements and automated NZ length measurements was $r = 0.9574$, with a coefficient of determination of $r^2 = 0.9166$ and $p < 0.001$, indicating strong correlation between manually determined and automated NZ length calculations (Fig. 5).

4. Discussion

Many different biomechanical protocols are used for IVD motion segment testing, and there lacks clarity on the testing protocols that are best able to detect injury effects on IVD biomechanical properties. This study showed that biomechanical properties determined from tests performed at lower magnitudes of axial preload and torsional rotation exhibited the largest differences between the intact and acute injury conditions. Torsional stiffness, torque range, and axial range of motion were the biomechanical parameters most sensitive to these defects. A minor injury was induced so that injury effects would be less pronounced between intact and injured IVDs, and therefore necessitate refined biomechanical testing methods to identify these differences. The capacity to detect subtly impaired biomechanical function is important clinically since these minor injuries might represent small AF tears, mild degenerative changes or repair progression following a regenerative medicine strategy. Large AF defects are known to have large effects on most axial and torsional biomechanical properties (Elliott et al., 2008), and do not require similar optimization of testing protocols for their detection.

Minor injuries had the largest effects on torsional stiffness, torque range and axial range of motion when these parameters were calculated from testing protocols at low axial amplitudes and preloads and at low rotational amplitudes. The sensitivity of torsional stiffness, torque range and axial range of motion parameters to injuries have been shown previously (Michalek et al., 2010a; Michalek and Iatridis, 2012; Krismer et al., 1996), but sensitivities to loading protocol have not. Parameters obtained under mild loading conditions appeared to best describe the ‘toe region’ or ‘neutral zone’ regions where relatively few annular fibers are recruited. Incision of AF fibers results in release of residual stress (Michalek et al., 2012), and these changes have the greatest influence on the toe region rather than the linear region. The effect of injury is largely dependent on the defect size or number of cut fibers (Elliott et al., 2008; Adams and Green, 1993), and these cut fibers may exert a greater influence on circumferential hoop-stresses, NP pressurization or outward bulging (Michalek et al., 2012) under mild loading conditions. In contrast, parameters obtained with high force axial preloads generate large hoop stresses that recruit a much larger number of AF fibers, most of which are intact, so that cut fibers from local needle puncture may have a relatively smaller influence. The composite nature of the highly fibrous AF structure has many levels of mechanical redundancy and even in the area of fiber damage neighboring fibers can be recruited to carry load adjacent to damaged fibers and damaged

fibers can carry also load a relatively short distance away from the fiber break (Iatridis and ap Gwynn, 2004). The most sensitive parameter to injury effects were torsional stiffness with low axial preloads, which is unsurprising since torsional testing with low axial preloads isolates the effects of AF fiber tension with fibers being stretched as rotation angle increases, since there is negligible NP pressurization.

There were some limitations of this study. Relatively high variability was observed in axial testing at low load magnitudes. Table 1 shows that the absolute variance is lower for the ± 1.6N test than for the higher loading magnitude tests. However, when normalized in Fig. 3, this variation is demonstrated to be a greater percentage of the mean. This pattern in variance is to be expected when testing over a large range of forces. Importantly, the statistical comparisons between load magnitude groups were on normalized data and accounted for this variance. In addition to the effects of varying loading protocols on biomechanical parameters, other factors such as motion segment hydration may play a role. Hydration has been shown to play an influential role on IVD compressive properties (Race et al., 2000), and could be considered as a variable in future studies aiming to optimize biomechanical testing protocols. Further, sequence of testing and load history from subsequent tests may influence biomechanical parameters and should be considered during loading protocol development (Costi et al., 2008; Amin et al., 2016).

The use of small animal models of IVD injury such as the rat is suitable for the assessment of AF repair, given the similarities biomechanical properties to human IVDs (Espinoza Orías et al., 2009; Beckstein et al., 2008; Elliott and Sarver, 2004; O'Connell et al., 2007), ease of implementation, and high repeatability. The rat tail IVD, when normalized for geometry, has similar biomechanical parameters compared to human lumbar IVDs (Showalter et al., 2012), and is a commonly used biomechanical model because tail IVDs are easily accessed for puncture and have axisymmetric geometry with relatively long vertebrae facilitating gripping, testing and analyses. The use of rat tail IVDs is also common in screening of biomaterial AF repair strategies *in vivo* (Sloan et al., 2017; Wang et al., 2017; Grunert et al., 2014, 2015; Borde et al., 2015), but IVD repair studies often lack biomechanical characterization. While some studies have assessed biomechanical changes immediately following rat IVD injury (Elliott et al., 2008; Michalek et al., 2010a), there is a paucity of literature. The 26G needle puncture is considered a minor injury as the defect (~40% IVD height) is localized to a single point and the majority of AF fibers remain intact. Future investigations are important to consider species differences since more fibrous NP regions of other species may exhibit some differences and since *ex vivo* and *in vivo* bovine, sheep, and goat which are important large animal models often required for translation of experimental AF repair strategies to the human. We observed that minor injury does not induce significant changes in hysteresis, yet the assessments of viscoelasticity are limited to this relatively high frequency testing. Stress relaxation and creep are additional tests used to calculate viscoelastic parameters at different time scales that are sensitive to IVD injury and repair (Sloan et al., 2017; Vresilovic et al., 2006) and warrant further investigation.

We further determined an automated NZ length measurement method that reduced analyses time and showed strong association with manually obtained NZ length values. Automated NZ length analyses could not be performed on axial force-displacement data due to

insufficient sampling rate, and axial NZ length was therefore measured manually. The automated method is an improvement to obtain NZ length measurements since it is an objective method without potential for operator bias, but is limited because it needs sufficient sampling rates to be applied.

In conclusion, the lowest axial loading magnitude of ± 1.6 N, the lowest compressive axial preload tested of −0.1 MPa, and the fewest degrees of rotation tested of ± 10° were the protocols that best detected effects of minor, acute injury in the rat tail IVD. There is no consensus on optimal biomechanical testing protocols even though axial and torsional biomechanical testing are an important functional outcome for characterizing injured and degenerated IVD motion segments, and for tracking success of IVD repair strategies. These findings highlight that minor injuries can be difficult to detect since they only disrupt relatively few fibers. Minor injury was easiest to detect when IVD biomechanical parameters were obtained under relatively mild axial load magnitudes, low axial preloads, and rotational amplitudes when parameters describe the ‘toe region’ portion of the curve where relatively few fibers are recruited and injury has the greatest effect. Mild loading conditions are also preferable since they are often less destructive if IVDs must undergo further assessments.

Acknowledgments

This work was supported by R01 R01AR057397 (JCI) from NIH/ NIAMS. We gratefully acknowledge Dr. Rose G. Long (Icahn School of Medicine at Mount Sinai, New York, NY) and Warren Hom (Icahn School of Medicine at Mount Sinai, New York, NY) for biomechanical testing and analysis assistance. The data in this paper were used in a dissertation as partial fulfillment of the requirements for a PhD degree at the Graduate School of Biomedical Sciences at Mount Sinai.

Abbreviations

AF	annulus fibrosus
IVD	intervertebral disc
NP	nucleus pulposus
ROM	range of motion
NZ	neutral zone

References

Adams MA, Dolan P, 2012 12 Intervertebral disc degeneration: evidence for two distinct phenotypes. J. Anat 221 (6), 497–506. [PubMed: 22881295]

Adams MA, Green TP, 1993 12 Tensile properties of the annulus fibrosus. I. The contribution of fibre-matrix interactions to tensile stiffness and strength. Eur. Spine J 2 (4), 203–208. [PubMed: 20058406]

Adams MA, Roughley PJ, 2006 8 15 What is intervertebral disc degeneration, and what causes it? Spine 31 (18), 2151–2161. [PubMed: 16915105]

Adams MA, McNally DS, Dolan P, 1996 11 “Stress” distributions inside intervertebral discs. The effects of age and degeneration. J. Bone Joint Surg. Br 78 (6), 965–972. [PubMed: 8951017]

Amin DB, Lawless IM, Sommerfeld D, Stanley RM, Ding B, Costi JJ, 2016 10 3 The effect of six degree of freedom loading sequence on the in-vitro compressive properties of human lumbar spine segments. J. Biomech 49 (14), 3407–3414. [PubMed: 27663622]

Beckstein JC, Sen S, Schaer TP, Vresilovic EJ, Elliott DM, 2008 3 Comparison of animal discs used in disc research to human lumbar. Disc. Spine 33 (6), E166–E173. [PubMed: 18344845]

Bezci SE, Klineberg EO, O'Connell GD, 2018 1 Effects of axial compression and rotation angle on torsional mechanical properties of bovine caudal discs. J. Mech. Behav. Biomed. Mater 77, 353–359. [PubMed: 28965042]

Borde B, Grunert P, Härtl R, Bonassar LJ, 2015 8 Injectable, high-density collagen gels for annulus fibrosus repair: an in vitro rat tail model. J. Biomed. Mater. Res. A 103 (8), 2571–2581. [PubMed: 25504661]

Carragee EJ, Don AS, Hurwitz EL, Cuellar JM, Carrino JA, Herzog R, 2009 10 1 2009 ISSLS Prize Winner: does discography cause accelerated progression of degeneration changes in the lumbar disc: a ten-year matched cohort study. Spine 34 (21), 2338–2345. [PubMed: 19755936]

Centers for Disease Control and Prevention (CDC), 2009 5 1 Prevalence and most common causes of disability among adults–United States, 2005. MMWR Morb. Mortal. Wkly. Rep 58 (16), 421–426. [PubMed: 19407734]

Cortes DH, Elliott DM, 2014 The intervertebral disc: overview of disc mechanics. In: Shapiro IM, Risbud MV(Eds.), The Intervertebral Disc: Molecular and Structural Studies of the Disc in Health and Disease, pp. 17–32.

Costi JJ, Stokes IA, Gardner-Morse M, Laible JP, Scoffone HM, Iatridis JC, 2007 1 2 Direct measurement of intervertebral disc maximum shear strain in six degrees of freedom: motions that place disc tissue at risk of injury. J. Biomech 40 (11), 2457–2466. [PubMed: 17198708]

Costi JJ, Stokes IA, Gardner-Morse MG, Iatridis JC, 2008 7 15 Frequency-dependent behavior of the intervertebral disc in response to each of six degree of freedom dynamic loading: solid phase and fluid phase contributions. Spine 33 (16), 1731–1738. [PubMed: 18628705]

GBD 2016 Disease and Injury Incidence and Prevalence Collaborators. Global, regional, and national incidence, prevalence, and years lived with disability for 328 diseases and injuries for 195 countries, 1990–2016: a systematic analysis for the Global Burden of Disease Study 2016. Lancet 390 (10100), 1211–1259.

Elliott DM, Sarver JJ, 2004 4 Young investigator award winner: validation of the mouse and rat disc as mechanical models of the human lumbar. Disc. Spine 29 (7), 713–722. [PubMed: 15087791]

Elliott DM, Yerramalli CS, Beckstein JC, Boxberger JI, Johannessen W, Vresilovic EJ, 2008 3 15 The effect of relative needle diameter in puncture and sham injection animal models of degeneration. Spine 33 (6), 588–596. [PubMed: 18344851]

Espinoza Orías AA, Malhotra NR, Elliott DM, 2009 3 Rat disc torsional mechanics: effect of lumbar and caudal levels and axial compression load. Spine J 9 (3), 204–209. [PubMed: 18495544]

Fazzalari NL, Costi JJ, Hearn TC, Fraser RD, Vernon-Roberts B, Hutchinson J, et al., 2001 12 1 Mechanical and pathologic consequences of induced concentric anular tears in an ovine model. Spine 26 (23), 2575–2581. [PubMed: 11725238]

Freemont AJ, Peacock TE, Goupille P, Hoyland JA, O'Brien J, Jayson MI, 1997 7 19 Nerve ingrowth into diseased intervertebral disc in chronic back pain. Lancet 350 (9072), 178–181. [PubMed: 9250186]

Gardner-Morse MG, Stokes IA, 2003 5 Physiological axial compressive preloads increase motion segment stiffness, linearity and hysteresis in all six degrees of freedom for small displacements about the neutral posture. J. Orthop. Res 21 (3), 547–552. [PubMed: 12706030]

Gardner-Morse MG, Stokes IAF, 2004 2 Structural behavior of human lumbar spinal motion segments. J. Biomech 37 (2), 205–212. [PubMed: 14706323]

Grunert P, Borde BH, Hudson KD, Macielak MR, Bonassar LJ, Härtl R, 2014 2 1 Annular repair using high-density collagen gel: a rat-tail in vivo model. Spine 39 (3), 198–206. [PubMed: 24253790]

Grunert P, Borde BH, Towne SB, Moriguchi Y, Hudson KD, Bonassar LJ, et al., 2015 10 Riboflavin crosslinked high-density collagen gel for the repair of annular defects in intervertebral discs: an in vivo study. Acta Biomater. 26, 215–224. [PubMed: 26116448]

Hampton D, Laros G, McCarron R, Franks D, 1989 4 Healing potential of the anulus fibrosus. Spine 14 (4), 398–401. [PubMed: 2718042]

Hartman RA, Bell KM, Quan B, Nuzhao Y, Sowa GA, Kang JD, 2015 4 Needle puncture in rabbit functional spinal units alters rotational biomechanics. J. Spinal Disord. Tech 28 (3), E146–E153. [PubMed: 25370985]

Hoy D, March L, Brooks P, Blyth F, Woolf A, Bain C, et al., 2014 6 The global burden of low back pain: estimates from the Global Burden of Disease 2010 study. Ann. Rheum. Dis 73 (6), 968–974. [PubMed: 24665116]

Hsieh AH, Hwang D, Ryan DA, Freeman AK, Kim H, 2009 5 1 Degenerative anular changes induced by puncture are associated with insufficiency of disc biomechanical function. Spine 34 (10), 998–1005. [PubMed: 19404174]

Iatridis JCJC, ap Gwynn I, 2004 8 Mechanisms for mechanical damage in the intervertebral disc annulus fibrosus. J. Biomech 37 (8), 1165–1175. [PubMed: 15212921]

Iatridis JC, Hecht AC, 2012 4 Commentary: does needle injection cause disc degeneration? News in the continuing debate regarding pathophysiology associated with intradiscal injections. Spine J 12 (4), 336–338. [PubMed: 22656311]

Iatridis JC, MacLean JJ, Roughley PJ, Alini M, 2006 4 Effects of mechanical loading on intervertebral disc metabolism in vivo. J. Bone Joint Surg. Am 88 (Suppl. 2), 41–46.

Iatridis JC, Michalek AJ, Purmessur D, Korecki CL, 2009 9 1 Localized intervertebral disc injury leads to organ level changes in structure, cellularity, and biosynthesis. Cell. Mol. Bioeng 2 (3), 437–447. [PubMed: 21179399]

Iatridis JC, Nicoll SB, Michalek AJ, Walter BA, Gupta MS, 2013 3 Role of biomechanics in intervertebral disc degeneration and regenerative therapies: what needs repairing in the disc and what are promising biomaterials for its repair? Spine J 13 (3), 243–262. [PubMed: 23369494]

Johannessen W, Cloyd JM, O'Connell GD, Vresilovic EJ, Elliott DM, 2006 4 Trans-endplate nucleotomy increases deformation and creep response in axial loading. Ann. Biomed. Eng 34 (4), 687–696. [PubMed: 16482409]

Krismer M, Haid C, Rabl W, 1996 11 15 The contribution of anulus fibers to torque resistance. Spine 21 (22), 2551–2557. [PubMed: 8961442]

Lai A, Moon A, Purmessur D, Skovrlj B, Winkelstein BA, Cho SK, et al., 2015 5 Assessment of functional and behavioral changes sensitive to painful disc degeneration. J. Orthop. Res 33 (5), 755–764. [PubMed: 25731955]

Livshits G, Popham M, Malkin I, Sambrook PN, Macgregor AJ, Spector T, et al., 2011 10 Lumbar disc degeneration and genetic factors are the main risk factors for low back pain in women: the UK Twin Spine Study. Ann. Rheum. Dis 70 (10), 1740–1745. [PubMed: 21646416]

Long RG, Torre OM, Hom WW, Assael DJ, Iatridis JC, 2016 2 Design requirements for annulus fibrosus repair: review of forces, displacements, and material properties of the intervertebral disk and a summary of candidate hydrogels for repair. J. Biomech. Eng 138 (2) 021007. [PubMed: 26720265]

Martin JT, Gorth DJ, Beattie EE, Harfe BD, Smith LJ, Elliott DM, 2013 8 Needle puncture injury causes acute and long-term mechanical deficiency in a mouse model of intervertebral disc degeneration. J. Orthop. Res 31 (8), 1276–1282. [PubMed: 23553925]

Masuda K, Aota Y, Muehleman C, Imai Y, Okuma M, Thonar EJ, et al., 2005 1 1 A novel rabbit model of mild, reproducible disc degeneration by an anulus needle puncture: correlation between the degree of disc injury and radiological and histological appearances of disc degeneration. Spine 30 (1), 5–14. [PubMed: 15626974]

Melrose J, Roberts S, Smith S, Menage J, Ghosh P, 2002 6 15 Increased nerve and blood vessel ingrowth associated with proteoglycan depletion in an ovine anular lesion model of experimental disc degeneration. Spine 27 (12), 1278–1285. [PubMed: 12065974]

Michalek AJ, Iatridis JC, 2012 5 22 Height and torsional stiffness are most sensitive to annular injury in large animal intervertebral discs. Spine J 12 (5), 425–432. [PubMed: 22627276]

Michalek AJ, Funabashi KL, Iatridis JC, 2010a 12 Needle puncture injury of the rat intervertebral disc affects torsional and compressive biomechanics differently. Eur. Spine J 19 (12), 2110–2116. [PubMed: 20544231]

Michalek AJ, Buckley MR, Bonassar LJ, Cohen I, Iatridis JC, 2010b 12 The effects of needle puncture injury on microscale shear strain in the intervertebral disc annulus fibrosus. Spine J 10 (12), 1098–1105. [PubMed: 20971041]

Michalek AJ, Gardner-Morse MG, Iatridis JC, 2012 4 30 Large residual strains are present in the intervertebral disc annulus fibrosus in the unloaded state. J. Biomech 45 (7), 1227–1231. [PubMed: 22342138]

Osti OL, Vernon-Roberts B, Moore R, Fraser RD, 1992 9 Annular tears and disc degeneration in the lumbar spine. A post-mortem study of 135 discs. J. Bone Joint Surg. Br 74 (5), 678–682. [PubMed: 1388173]

O'Connell GD, Vresilovic EJ, Elliott DM, 2007 2 1 Comparison of animals used in disc research to human lumbar disc geometry. Spine 32 (3), 328–333. [PubMed: 17268264]

O'Connell GD, Vresilovic EJ, Elliott DM, 2011 4 Human intervertebral disc internal strain in compression: the effect of disc region, loading position, and degeneration. J. Orthop. Res 29 (4), 547–555. [PubMed: 21337394]

Panjabi MM, 1992 12 The stabilizing system of the spine. Part II. Neutral zone and instability hypothesis. J. Spinal Disord 5 (4), 390–396 discussion 397. [PubMed: 1490035]

Race A, Broom ND, Robertson P, 2000 3 15 Effect of loading rate and hydration on the mechanical properties of the disc. Spine 25 (6), 662–669. [PubMed: 10752096]

Rousseau M-AA, Ulrich JA, Bass EC, Rodriguez AG, Liu JJ, Lotz JC, 2007 1 1 Stab incision for inducing intervertebral disc degeneration in the rat. Spine 32 (1), 17–24. [PubMed: 17202887]

Showalter BL, Beckstein JC, Martin JT, Beattie EE, Espinoza Orías AA, Schaer TP, et al., 2012 7 1 Comparison of animal discs used in disc research to human lumbar disc: torsion mechanics and collagen content. Spine 37 (15), E900–E907. [PubMed: 22333953]

Sloan SR, Galesso D, Secchieri C, Berlin C, Hartl R, Bonassar LJ, 2017 9 1Initial investigation of individual and combined annulus fibrosus and nucleus pulposus repair ex vivo. Acta Biomater. 59, 192–199. [PubMed: 28669721]

Sloan SR, Lintz M, Hussain I, Hartl R, Bonassar LJ, 2018 1 11 Biologic annulus fibrosus repair: a review of preclinical in vivo investigations. Tissue Eng. B Rev. 24 (3), 179–190.

Sobajima S, Kompel JF, Kim JS, Wallach CJ, Robertson DD, Vogt MT, et al., 2005 1 1 A slowly progressive and reproducible animal model of intervertebral disc degeneration characterized by MRI, X-ray, and histology. Spine 30 (1), 15–24. [PubMed: 15626975]

Thompson RE, Pearcy MJ, Downing KJ, Manthey BA, Parkinson IH, Fazzalari NL, 2000 12 1 Disc lesions and the mechanics of the intervertebral joint complex. Spine 25 (23), 3026–3035. [PubMed: 11145814]

Thompson RE, Pearcy MJ, Barker TM, 2004 6 The mechanical effects of intervertebral disc lesions. Clin. Biomech 19 (5), 448–455.

Torre OM, Das R, Berenblum RE, Huang AH, Iatridis JC, 2018 3 23 Neonatal mouse intervertebral discs heal with restored function following herniation injury. FASEB J 32 (9), 4753–4762 fj201701492R. [PubMed: 29570392]

Ulrich JA, Liebenberg EC, Thuillier DU, Lotz JC, 2007 12 1 ISSLS prize winner: repeated disc injury causes persistent inflammation. Spine 32 (25), 2812–2819. [PubMed: 18246002]

van Heeswijk VM, Thambyah A, Robertson PA, Broom ND, 2018 4 1 Does an annular puncture influence the herniation path?: an in vitro mechanical and structural investigation. Spine 43 (7), 467–476. [PubMed: 28719550]

Vresilovic EJ, Johannessen W, Elliott DM, 2006 12 Disc mechanics with trans-endplate partial nucleotomy are not fully restored following cyclic compressive loading and unloaded recovery. J. Biomech. Eng 128 (6), 823–829. [PubMed: 17154681]

Wang Y, Wang X, Shang J, Liu H, Yuan Y, Guo Y, et al., 2017 Repairing the ruptured annular fibrosus by using type I collagen combined with citric acid, EDC and NHS: an in vivo study. Eur. Spine J 26 (3), 884–893. [PubMed: 28004245]

Wilke HJ, Neef P, Caimi M, Hoogland T, Claes LE, 1999 4 15 New in vivo measurements of pressures in the intervertebral disc in daily life. Spine 24 (8), 755–762. [PubMed: 10222525]

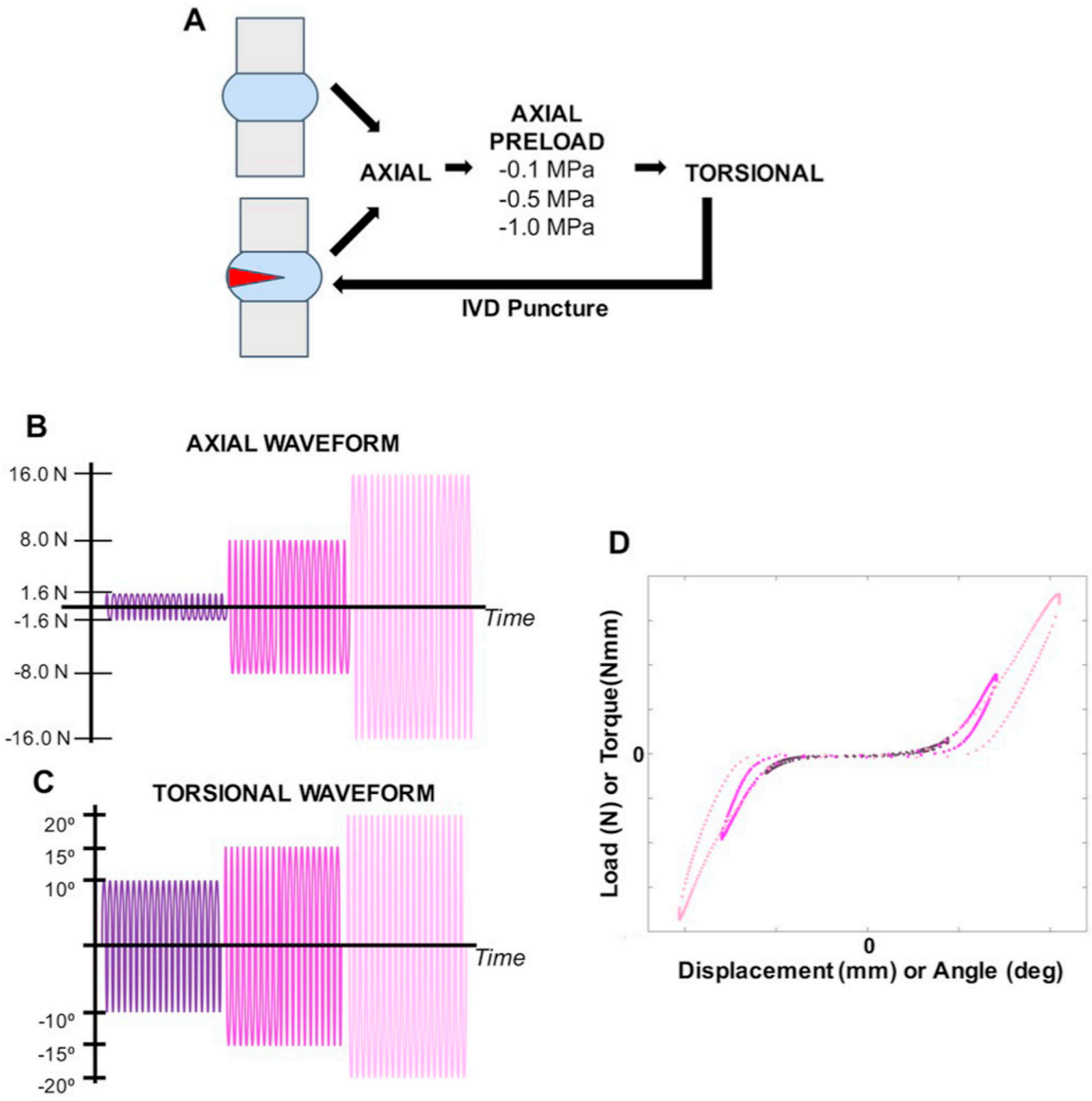

Fig. 1.

Biomechanical test protocols. A) A repeated measures study design to determine effects of acute injury on rat tail IVD mechanical parameters. B) Axial tension-compression testing was performed with a stress sweep of 20 cycles per sweep at ± 1.6N, ± 8.0N, and ± 16.0N. C) Torsional testing was performed with a rotation angle sweep of 20 cycles per sweep at ± 10°, ± 15°, and ± 20°. D) Representative force vs. displacement loading curves for intact and acutely injured samples demonstrate the parameters obtained including axial ROM, tensile stiffness, and compressive stiffness.

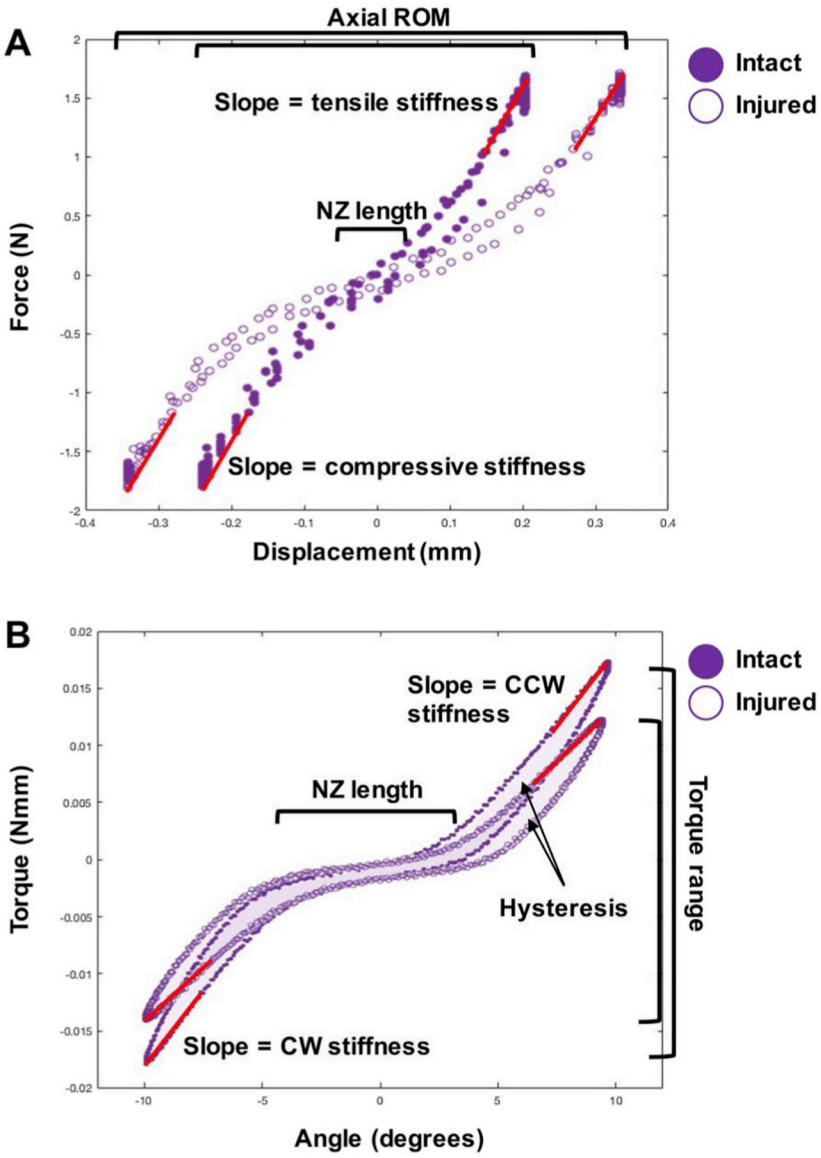

Fig. 2.

Intact and injured loading curved from axial and torsional testing. A) Representative axial force-displacement curve for intact and acutely injured samples demonstrate parameters obtained including axial range of motion (ROM), tensile stiffness, compressive stiffness and NZ length. B) Representative torsional torque-angle loading curves for intact and acutely injured samples demonstrate the torque range, NZ length, hysteresis, and torsional stiffness (taken as the average of CCW and CW stiffnesses).

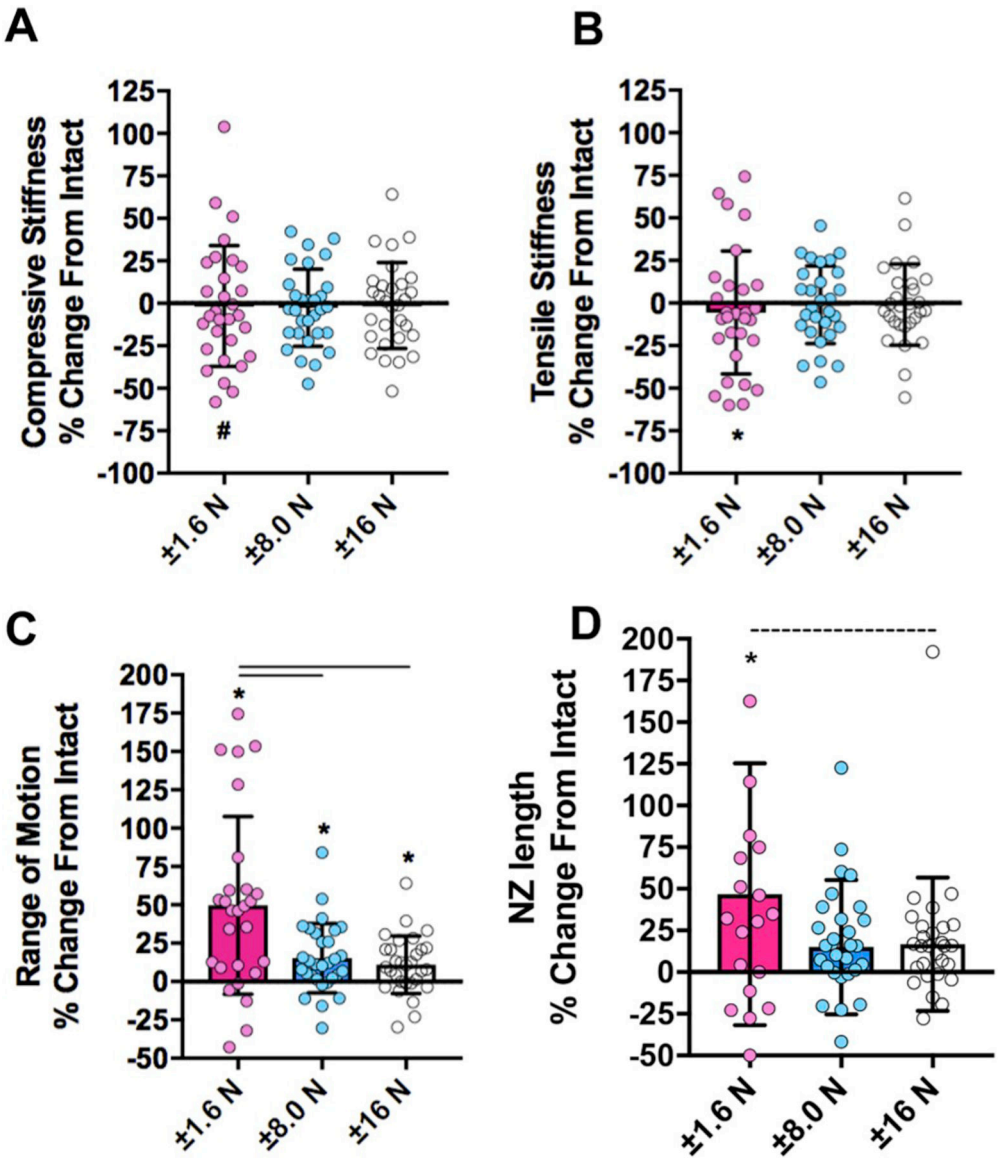

Fig. 3.

Percent change of axial mechanical parameters demonstrated that low loading magnitude amplifies differences in axial properties after mild injury. A,B) Compressive stiffness and tensile stiffness decreased only at the lowest loading magnitude. C) Axial range of motion increased in all loading groups, but the effect was amplified by the lowest loading magnitude. D) Axial NZ length increased following injury at the lowest loading magnitude. *$p < 0.05$ between intact and injury. Solid bars $p < 0.05$, dashed bar $p < 0.1$ (trend) between loading magnitudes. Data presented as mean ± standard deviation (SD).

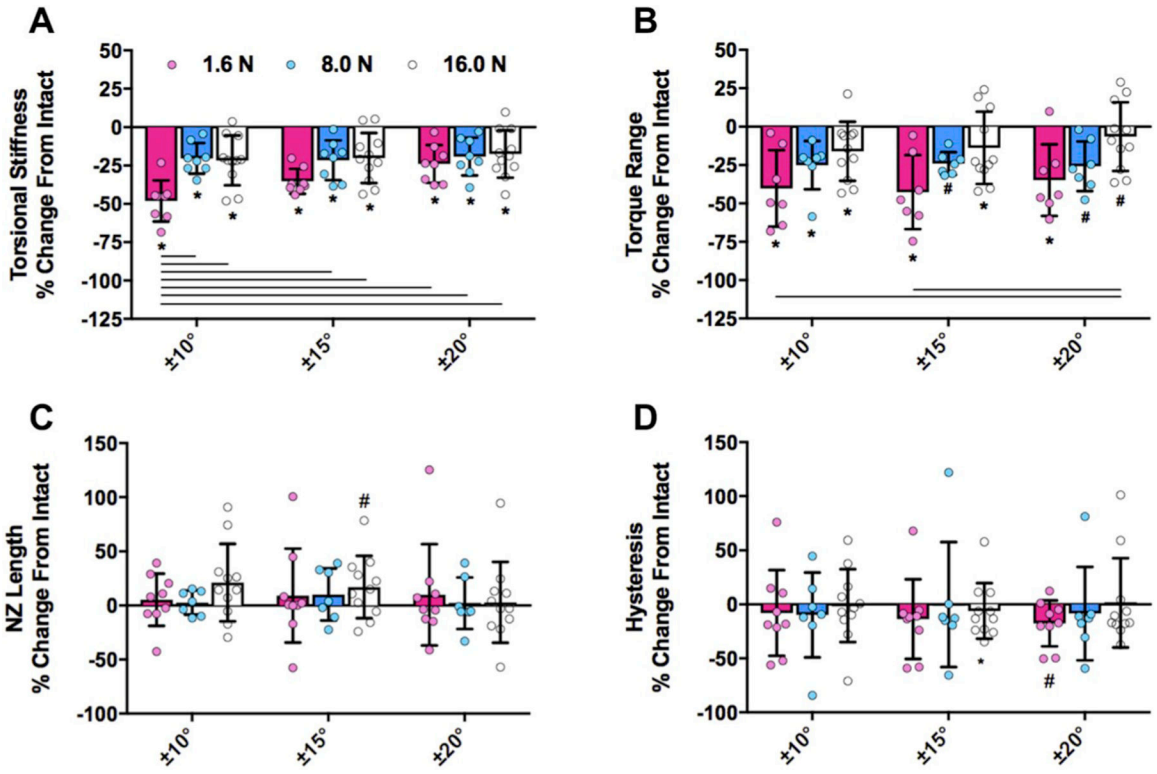

Fig. 4.

Percent change of torsional mechanical parameters demonstrated that low loading magnitude amplifies differences in torsional properties after mild injury. A,B) Torsional stiffness and torque range decreased following injury, and this effect was amplified at the lowest axial preload combined with the fewest degrees of rotation. C,D) Torque range and hysteresis were highly variable and mostly insensitive to acute injury. *$p < 0.05$, #$p < 0.1$ (trend) between intact and injury. Bars $p < 0.05$ between loading magnitudes. Data presented as mean ± standard deviation (SD).

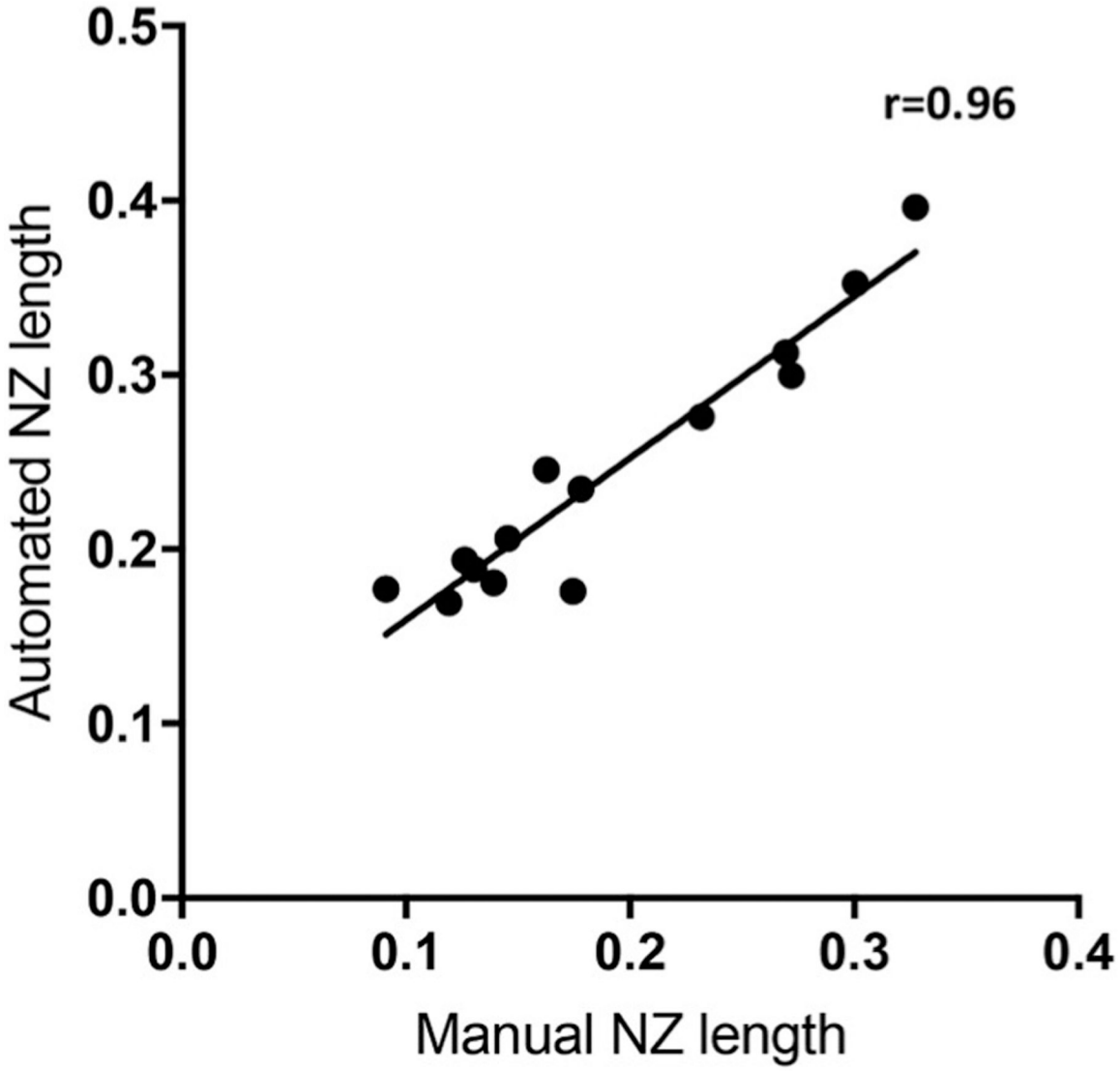

Fig. 5.
Correlation of automated NZ length and manual NZ length measurements. 14 samples were randomly selected for comparison and demonstrated a strong association (r = 0.96).

Table 1

Parameter	Intact	Injury	% Change
Compressive Stiffness (N/mm)			
± *1.6 N*	14.26 (4.44)	12.96 (3.15)	−1.58 (35.46)
± *8.0 N*	58.98 (13.64)	56.06 (13.09)	−2.62 (22.67)
± *16.0 N*	89.09 (32.01)	86.07 (30.71)	−1.24 (25.28)
Tensile Stiffness (N/mm)			
± *1.6 N*	12.22 (3.13)	10.78 (3.20)	−5.94 (35.56)
± *8.0 N*	49.92 (11.68)	47.90 (11.46)	−1.63 (22.73)
± *16.0 N*	66.38 (30.97)	66.73 (24.19)	4.07 (25.68)
Range of Motion (mm)			
± *1.6 N*	0.45 (0.23)	0.57 (0.19)	49.18 (75.29)
± *8.0 N*	0.87 (0.20)	0.98 (0.18)	15.25 (22.62)
± *16.0 N*	1.18 (0.28)	1.28 (0.24)	10.93 (18.80)
Neutral Zone Length (mm)			
± *1.6 N*	0.27 (0.13)	0.35 (0.16)	46.8 (78.6)
± *8.0 N*	0.60 (0.17)	0.66 (0.21)	15.0 (40.3)
± *16.0 N*	0.77 (0.33)	0.82 (0.16)	16.7 (40.0)

Table 2

Parameter	Intact	Injury	% Change
Torsional Stiffness (Nmm/rad)			
± *1.6 N*			
± 10^0	0.26 (0.11)	0.16 (0.08)	−34.1 (26.4)
± 15^0	0.33 (0.12)	0.24 (0.11)	−26.3 (21.3)
± 20^0	0.34 (0.12)	0.28 (0.12)	−15.0 (21.2)
± *8.0 N*			
± 10^0	0.30 (0.13)	0.24 (0.12)	−20.3 (9.9)
± 15^0	0.34 (0.14)	0.27 (0.13)	−21.5 (13.0)
± 20^0	0.36 (0.14)	0.30 (0.14)	−19.2 (12.3)
± *16.0 N*			
± 10^0	0.31 (0.15)	0.24 (0.13)	−20.6 (19.0)
± 15^0	0.35 (0.19)	0.29 (0.18)	−19.4 (18.3)
± 20^0	0.38 (0.20)	0.34 (0.25)	−18.0 (17.0)
Torque Range (Nmm)			
± *1.6 N*			
± 10^0	0.037 (0.013)	0.031 (0.022)	−14.0 (47.6)
± 15^0	0.078 (0.029)	0.059 (0.038)	−24.7 (42.8)
± 20^0	0.113 (0.037)	0.092 (0.056)	−18.2 (34.9)
± *8.0 N*			
± 10^0	0.066 (0.020)	0.052 (0.020)	−21.2 (18.0)
± 15^0	0.095 (0.035)	0.080 (0.029)	−12.0 (34.5)
± 20^0	0.128 (0.044)	0.107 (0.042)	−15.1 (33.6)
± *16.0 N*			
± 10^0	0.076 (0.036)	0.060 (0.022)	−11.1 (19.6)
± 15^0	0.109 (0.048)	0.087 (0.033)	−9.3 (26.6)
± 20^0	0.135 (0.065)	0.122 (0.062)	−2.4 (24.9)

Table 3

Parameter	Intact	Injury	% Change
NZ Length (rad)			
± *1.6 N*			
± 10^0	0.16 (0.02)	0.17 (0.04)	5.3 (24.2)
± 15^0	0.21 (0.04)	0.22 (0.07)	9.1 (43.4)
± 20^0	0.25 (0.05)	0.26 (0.07)	9.9 (46.9)
± *8.0 N*			
± 10^0	0.13 (0.05)	0.13 (0.04)	6.9 (25.3)
± 15^0	0.16 (0.03)	017 (0.01)	10.2 (24.0)
$\pm 20^0$	0.23 (0.06)	0.23 (0.03)	2.1 (23.8)
± *16.0 N*			
± 10^0	0.09 (0.04)	0.10 (0.02)	3.6 (22.0)
± 15^0	0.13 (0.02)	0.15 (0.03)	17.1 (28.9)
$\pm 20^0$	0.21 (0.07)	0.20 (0.06)	2.9 (37.4)
Hysteresis (Nmm*rad)			
± *1.6 N*			
± 10^0	0.0006 (0.0003)	0.0005 (0.0004)	−8.0 (39.7)
± 15^0	0.0015 (0.0006)	0.0013 (0.0009)	−13.7 (36.9)
$\pm 20^0$	0.0031 (0.0012)	0.0026 (0.0014)	−17.5 (21.2)
± *8.0 N*			
± 10^0	0.0015 (0.0006)	0.0012 (0.0004)	−8.1 (42.4)
± 15^0	0.0027 (0.0006)	0.0024 (0.0009)	−0.3 (57.8)
± 20^0	0.0047 (0.0010)	0.0042 (0.0016)	−8.5 (43.2)
± *16.0 N*			
± 10^0	0.0020 (0.0010)	0.0017 (0.0005)	−2.6 (37.9)
± 15^0	0.0033 (0.0012)	0.0029 (0.0008)	−6.0 (25.7)
± 20^0	0.0053 (0.0022)	0.0049 (0.0018)	1.4 (41.3)